Inspiratory bursts in the preBötzinger complex depend on a calcium-activated non-specific cation current linked to glutamate receptors in neonatal mice

Ryland W. Pace[1], Devin D. Mackay[2], Jack L. Feldman[2] and Christopher A. Del Negro[1,2]

[1]*Department of Applied Science, McGlothlin-Street Hall, Room 303, The College of William and Mary, Williamsburg, VA 23187-8795, USA*
[2]*Systems Neurobiology Laboratory, Department of Neurobiology, David Geffen School of Medicine at the University of California Los Angeles, Box 951763, Los Angeles, CA 90095-1763, USA*

Inspiratory neurons of the preBötzinger complex (preBötC) form local excitatory networks and display 10–30 mV transient depolarizations, dubbed *inspiratory drive potentials*, with superimposed spiking. AMPA receptors are critical for rhythmogenesis under normal conditions *in vitro* but whether other postsynaptic mechanisms contribute to drive potential generation remains unknown. We examined synaptic and intrinsic membrane properties that generate inspiratory drive potentials in preBötC neurons using neonatal mouse medullary slice preparations that generate respiratory rhythm. We found that NMDA receptors, group I metabotropic glutamate receptors (mGluRs), but not group II mGluRs, contributed to inspiratory drive potentials. Subtype 1 of the group I mGluR family (mGluR1) probably regulates a K^+ channel, whereas mGluR5 operates via an inositol 1,4,5-trisphosphate (IP_3) receptor-dependent mechanism to augment drive potential generation. We tested for and verified the presence of a Ca^{2+}-activated non-specific cation current (I_{CAN}) in preBötC neurons. We also found that high concentrations of intracellular BAPTA, a high-affinity Ca^{2+} chelator, and the I_{CAN} antagonist flufenamic acid (FFA) decreased the magnitude of drive potentials. We conclude that I_{CAN} underlies robust inspiratory drive potentials in preBötC neurons, and is only fully evoked by ionotropic and metabotropic glutamatergic synaptic inputs, i.e. by network activity.

(Resubmitted 29 March 2007; accepted 17 April 2007; first published online 19 April 2007)
Corresponding author C. A. Del Negro: Department of Applied Science, McGlothlin-Street Hall, Room 303, The College of William and Mary, Williamsburg, VA 23187-8795, USA. Email: cadeln@wm.edu

Neurons in the preBötzinger complex (preBötC) of the ventrolateral medulla synchronously produce 300–500 ms bursts during the inspiratory phase of the respiratory cycle *in vitro* (for review see Feldman & Del Negro, 2006). Each inspiratory burst in a single neuron is characterized by action potentials superimposed on a 10–30 mV envelope of depolarization, i.e. *inspiratory drive potential*. Less than 20% of neonatal preBötC neurons express intrinsic bursting properties, i.e. *pacemaker* properties, *in vitro* (Peña *et al.* 2004; Del Negro *et al.* 2005). Therefore, most preBötC neurons generate inspiratory drive potentials by synaptic input evoking postsynaptic currents that depend on intrinsic membrane properties.

AMPA receptors (AMPARs) are critical for production of inspiratory drive potentials *in vitro* (Greer *et al.* 1991; Funk *et al.* 1993; Ge & Feldman, 1998; Koshiya & Smith, 1999). However, AMPARs rapidly and strongly desensitize (Trussell & Fischbach, 1989; Patneau *et al.* 1992; Trussell *et al.* 1993; Attwell & Gibb, 2005), which affects inspiratory rhythm (Funk *et al.* 1995) and probably limits the contribution of AMPARs in inspiratory drive potential generation. Therefore, we posit that under normal circumstances other postsynaptic mechanisms, such as those associated with NMDA receptors (NMDARs) and metabotropic glutamate receptors (mGluRs), are linked to the activation of intrinsic conductances that play an integral role in inspiratory drive potential generation, an idea introduced by Rekling and colleagues (Rekling *et al.* 1996; Rekling & Feldman, 1998; Feldman & Del Negro, 2006).

Both NMDARs and group I mGluRs contribute to burst-like discharges associated with Purkinje neuron slow EPSPs (Canepari *et al.* 2001), neocortical epileptiform discharges (Schiller, 2004), and subthalamic neuron rhythmic bursting (Zhu *et al.* 2004*a*,*b*). NMDARs are widely expressed in preBötC neurons (Funk *et al.* 1993, 1997; Paarmann *et al.* 2000, 2005) and mGluRs, notably

This paper has online supplemental material.

 DOI: 10.1113/jphysiol.2007.133660

groups I and III, are also present (Mironov & Richter, 2000; Lieske & Ramirez, 2006; Ruangkittisakul *et al.* 2006). Although the roles of these glutamate receptors in the generation of respiratory motor output in *en bloc* and slice preparations *in vitro* have been examined, the contributions of NMDARs and mGluRs to inspiratory drive potential generation in preBötC neurons remains to be thoroughly investigated.

We hypothesized (Feldman & Del Negro, 2006) that intrinsic conductances such as the persistent sodium current (I_{NaP}) (Del Negro *et al.* 2002*a*,*b*) and the calcium-activated non-specific cation current (I_{CAN}) (Peña *et al.* 2004; Del Negro *et al.* 2005) are normally evoked by, and augment, synaptic input, which underlies the inspiratory drive potential (Rekling & Feldman, 1998; Feldman & Del Negro, 2006). Recently, we demonstrated that I_{NaP} does not contribute to inspiratory drive potential generation in the vast majority of preBötC neurons (Pace *et al.* 2007). However, the role of I_{CAN} remains largely speculative. I_{CAN} activation can be triggered by either NMDARs (Zhu *et al.* 2004*a*,*b*) or group I mGluRs (Congar *et al.* 1997; Partridge & Valenzuela, 1999), which makes it a candidate for amplifying glutamatergic synaptic drive by utilizing NMDAR-mediated Ca^{2+} flux and mGluR- and IP_3-mediated intracellular Ca^{2+} release to directly gate I_{CAN} and cause postsynaptic potentials.

We tested the role of non-AMPA postsynaptic glutamate receptors in drive potential generation. NMDARs and group I mGluRs, but not group II mGluRs, contribute substantially to inspiratory drive potentials. We found that the subtype 5 of the group I mGluRs (mGluR5) leads to inositol 1,4,5-trisphosphate (IP_3) receptor (IP_3R) activation. Our findings suggest that postsynaptic Ca^{2+} transients induced by glutamatergic transmission normally recruit I_{CAN} to amplify synaptic currents to generate robust inspiratory drive potentials.

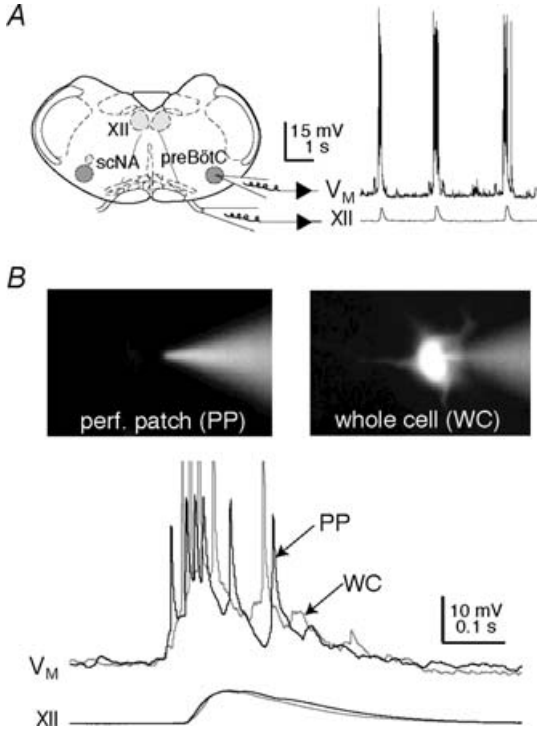

Figure 1. The slice preparation and experimental methodology
A, schematic depiction of the transverse slice preparation, illustrating bilateral preBötC and XII motor nuclei (XII), as well as the semicompact division of the nucleus ambiguous (scNA). Patch and suction electrodes are also illustrated. Recordings of the intracellular voltage trajectory of a preBötC neuron (V_M) and the integrated XII motor output are shown for three cycles of inspiratory activity. *B*, perforated-patch and whole-cell recordings. The perforated-patch configuration (PP; left panel) is confirmed by the failure of the Lucifer yellow in the patch-pipette solution to dialyse the neuron. The whole-cell configuration (WC; right panel) allows Lucifer yellow to fill the neuron. The voltage traces shown below verify that the underlying depolarization of the inspiratory burst, i.e. the inspiratory drive potential, can be accurately measured in PP mode as compared to the first minute of WC mode. Baseline membrane potential was –60 mV.

Methods

We used neonatal C57BL/6 mice aged 0–6 days (P0–6) for experiments *in vitro*. The Office for the Protection of Research Subjects (University of California Animal Research Committee) and the Institutional Animal Care and Use Committee (The College of William and Mary) approved all protocols.

Neonatal mice were anaesthetized using hypothermia and then rapidly decerebrated. The neuraxis was dissected in normal artificial cerebrospinal fluid (ACSF) containing (mM): 124 NaCl, 3 KCl, 1.5 $CaCl_2$, 1 $MgSO_4$, 25 $NaHCO_3$, 0.5 NaH_2PO_4, and 30 D-glucose, equilibrated with 95% O_2 and 5% CO_2 with pH = 7.4. Using a vibrating microslicer and landmark criteria recently characterized via an online histology atlas (Ruangkittisakul *et al.* 2006), we cut transverse slices (550 μm thick, Fig. 1*A*) that contained the preBötC at the rostral surface and hypoglossal (XII) motoneurons. The rostral cut captured the rostral-most XII nerve roots, the dorsomedial cell column and principal lateral loop of the inferior olivary nucleus, which places the preBötC at or near the rostral surface (Ruangkittisakul *et al.* 2006). The caudal cut captured the obex.

Slices were perfused with 27°C ACSF at 4 ml min^{-1} in a 0.5 ml chamber mounted rostral side up in a fixed-stage microscope equipped with Koehler illumination, infrared-enhanced differential interference contrast videomicroscopy and epifluorescence. ACSF K^+ concentration was raised to 9 mM and respiratory motor output was recorded from XII nerve roots using suction electrodes and a differential amplifier. The XII discharge was conditioned using a true RMS-to-DC converter (Analog Devices, One Technology Way, Norwood, MA, USA), which produces a full-wave rectified and smoothed

XII waveform (e.g. XII trace in Fig. 1*A*) based on the root-mean-square of voltage input to the differential amplifier (Dagan Instruments, Minneapolis, MN, USA).

All electrical recordings were performed on inspiratory preBötC neurons, visually localized ventral to the semicompact division of the nucleus ambiguous (Fig. 1*A*), which exhibited an inspiratory discharge pattern (Fig. 1*A*). We did not attempt to identify neurons with pacemaker properties and discarded recordings from expiratory neurons. Current-clamp recordings were performed using a Dagan IX2-700 amplifier. Data were digitally acquired at 4–20 kHz using a 16-bit A/D converter after low-pass filtering at 1 kHz to avoid aliasing. Intracellular pipettes (with 3–4 MΩ resistance) were fabricated from capillary glass (o.d., 1.5 mm; i.d., 0.87 mm) and filled with one of three different intracellular solutions. Standard potassium gluconate solution contained (mM): 140 potassium gluconate, 5 NaCl, 0.1 EGTA, 10 Hepes, 2 Mg-ATP, and 0.3 Na-GTP. Second, a Cs^+-based solution contained: 140 caesium gluconate (or caesium methane sulphonate), 10 NaCl, 1.5 BAPTA (tetra-acetic acid), 10 Hepes, 0.7 $CaCl_2$, 2 Mg-ATP, and 0.3 Na-GTP. Third, 30 mM BAPTA solution contained: 30 K_4-BAPTA, 20 potassium gluconate, 10 NaCl, 10 Hepes, 2 $MgCl_2$, 50 sucrose, and 0.3 Na-GTP. The K_4-BAPTA-based patch solution contained either $CaCl_2$ or $Ca(CF_3SO_3)_2$ to buffer the steady-state intracellular Ca^{2+} concentration (i.e. $[Ca^{2+}]_i$). To obtain nominally 0 nM $[Ca^{2+}]_i$ we added nothing, for 25 nM $[Ca^{2+}]_i$ we added 1.6 mM $CaCl_2$, and for 120 nM $[Ca^{2+}]_i$ we added 6 mM $Ca(CF_3SO_3)_2$ according to calculations by Maxchelator/WebMaxC software for determining the free metal concentration in the presence of chelators (www.stanford.edu/~cpatton/maxc.html). The liquid junction potentials of the potassium gluconate (8 mV), Cs^+-based patch (3 mV), and BAPTA-based (8 mV) patch solutions were corrected offline.

In current clamp, we continuously monitored membrane potential and adjusted the bias current to maintain a baseline membrane potential of −60 mV to provide a uniform standard for comparison of drive potentials among preBötC neurons. In some experiments using Cs^+-based patch solution, endogenous EPSPs generated plateau potentials during the interburst interval when baseline membrane potential was held at −60 mV. In these experiments baseline membrane potential was held at −80 mV so that plateau-like inspiratory potentials occurred only during the inspiratory phase.

We applied drugs such as xestospongin-C (Xes) and BAPTA (Sigma-Aldrich, St Louis, MO, USA) intracellularly through the patch pipette solution. Xes was added to the standard potassium gluconate patch solution immediately prior to use and discarded after 2 h. We used nystatin perforated patches to obtain baseline control data after obtaining a gigaohm seal and prior to intracellular drug application (Sakmann & Neher, 1995). Nystatin (250 μg ml^{-1}) was added to the patch solution immediately prior to use. To verify the integrity of the patch, we backfilled our pipettes with a patch solution containing 0.5% Lucifer yellow. After ~20 min of exposure to nystatin the amplitude and area of the underlying inspiratory drive potentials could be accurately measured, even though the high-impedance of the perforated patch partially attenuated action potentials. Fluorescence was confined to the pipette in this condition (Fig. 1*B*). Subsequently, the patch solution containing BAPTA or Xes was delivered intracellularly via patch rupture, which dialysed the cytosol and filled the neuron with fluorescent dye reflecting the whole-cell configuration (Fig. 1*B*).

We bath-applied these drugs obtained from Sigma-Aldrich: flufenamic acid (FFA), and DL-2-amino-5-phosphonovaleric acid (APV). We obtained tetrodotoxin (TTX) from EMD Biosciences (San Diego, CA, USA). (*RS*)-1-Amino-5-phosphonoindan-1-carboxylic acid (APICA), 6-methyl-2-(phenylethynyl)pyridine hydrochloride (MPEP), and (*S*)-(+)-amino-4-carboxy-2-methylbenzeneacetic acid (LY367385) were obtained from Tocris Bioscience (Ellisville, MO, USA). We substituted choline for Na^+ in some experiments (Fig. 8*B–D*) thus the ACSF contained (mM): 124 choline chloride, 9 KCl, 25 choline bicarbonate, 30 D-glucose, 1.5 $CaCl_2$ and 1 $MgSO_4$. $H_2PO_4^-$ was omitted to prevent precipitation.

Respiratory period *in vitro* was computed from the average of 10 consecutive inter-inspiratory burst intervals, where each cycle was triggered by XII motor output. We measured the amplitude and area of inspiratory drive potentials and XII motor output. The inspiratory drive potential, i.e. the envelope of depolarization that underlies spike bursts during the inspiratory phase, was obtained by digitally filtering the intracellular voltage trajectory to remove spikes but preserve the amplitude and area of the underlying voltage trajectory. The mean drive potential and XII motor output were computed by averaging 10 consecutive cycles. We compared all of these measures in control and in the presence of various drugs using paired *t* tests or an analysis of variance (ANOVA, Fig. 6*D*), with significance for the two-tailed test set at a minimum of $P < 0.05$.

Results

Rhythmically active preBötC neurons generate inspiratory bursts that collectively drive inspiratory motor output. Medullary slice preparations that retain the preBötC generate inspiratory rhythm and motor output that can be monitored via the XII nerve roots (Smith *et al.* 1991), while providing optimal experimental access to preBötC neurons. We tested the roles of postsynaptic conductances

in shaping the inspiratory drive potentials that underlie inspiratory bursts in rhythmically active preBötC neurons. Left unperturbed, inspiratory drive potentials and XII motor output normally remain stable for 60–80 min (see Figure S1 in online Supplemental material).

Role of glutamatergic synaptic input in preBötC neurons

We tested the NMDAR contribution using the antagonist APV (30–50 μM, bath-applied for >20 min), which significantly decreased the amplitude and area of drive potentials to $79 \pm 4\%$ and $76 \pm 2\%$ of control (both $P < 0.05$). APV had a negligible effect on the amplitude ($93 \pm 12\%$ of control), area ($91 \pm 2\%$), and frequency ($88 \pm 2\%$) of XII discharge (all $P > 0.17$, $n = 5$, Fig. 2*A*).

PreBötC neurons express mGluRs (Mironov & Richter, 2000; Lieske & Ramirez, 2006; Ruangkittisakul *et al.* 2006). Group III mGluRs are typically presynaptic (Stuart *et al.* 1999; Ferraguti & Shigemoto, 2006; Lieske & Ramirez, 2006) so we focused on the postsynaptic roles of groups I and II.

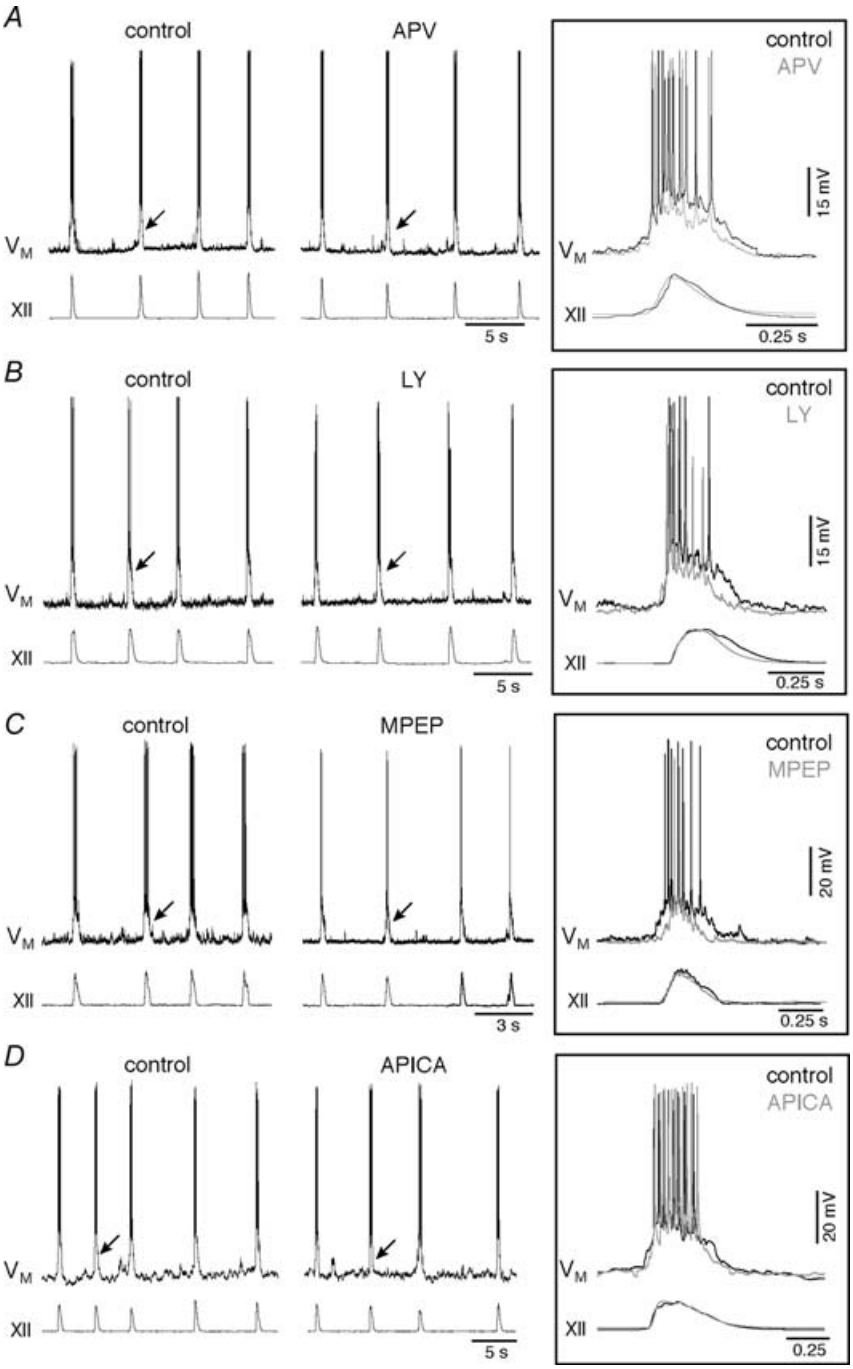

Figure 2. Effects of bath applications of non-AMPA glutamate receptor antagonists on drive potential generation and XII motor output
A, APV (50 μM) attenuates inspiratory bursts, but has no effect on XII motor output. *B*, the mGluR1 antagonist LY367385 (LY; 15 μM) attenuates inspiratory bursts, but has no effect on XII motor output. *C*, the mGluR5 antagonist MPEP (10 μM) attenuates inspiratory bursts, but has no effect on XII motor output. *D*, the general group II mGluR antagonist APICA (300 μM) significantly reduces the frequency of XII motor output but has no effect on inspiratory bursts. In *A–D*, arrows indicate inspiratory bursts shown at high time resolution in the insets at right. Voltage calibration bars in the insets apply to all traces in *A–D*. Individual time calibration bars are illustrated for traces and insets. Baseline membrane potential was −60 mV.

Group I includes subtypes 1 and 5 (mGluR1 and mGluR5). Bath-application of the specific mGluR1 antagonist LY367385 (LY; 15 μM, > 15 min) significantly reduced drive potential amplitude and area to 84 ± 4% and 73 ± 8% of control (both $P < 0.05$, $n = 5$). LY had no effect on the amplitude (99 ± 8% of control), area (104 ± 8%), or frequency (97 ± 4%) of XII motor output (all $P > 0.6$, $n = 9$, Fig. 2*B*). Similarly, bath-application of MPEP (10 μM, > 15 min), a selective mGluR5 antagonist, significantly reduced drive potential amplitude and area to 76 ± 4% and 61 ± 4% of control (both $P < 0.01$). MPEP had no effect on the amplitude (95 ± 5% of control), area (79 ± 5%), or frequency (103 ± 13%) of XII motor output (all $P > 0.14$, $n = 7$, Fig. 2*C*). These results suggest that both mGluR1 and mGluR5 contribute to inspiratory drive potential generation that is without effect on frequency or amplitude of motor output.

We also tested the role of group II mGluRs using bath application of the general group II antagonist APICA (300 μM, > 20 min). APICA had no significant effect on the amplitude (90 ± 7% of control) or area (90 ± 9%) of the drive potential (both $P > 0.3$), nor had any effect on the amplitude (102 ± 4%) or area (107 ± 10%) of the XII motor output (both $P > 0.5$). However, APICA significantly reduced the frequency of XII motor output to 88 ± 4% of control ($P < 0.05$, $n = 4$, Fig. 2*D*). These findings suggest that group II mGluRs can affect respiratory frequency without an obligatory change in inspiratory drive potential generation in preBötC neurons.

Mechanisms of group I mGluRs

By what mechanisms do group I mGluRs contribute to inspiratory drive potentials? Group I mGluRs are linked to L-type Ca^{2+} channel regulation in preBötC neurons (Mironov & Richter, 2000) so we tested the contribution of these channels. Bath-applied nifedipine (NIF, 10 μM, > 15 min) had no significant effect on drive potentials: amplitude (97 ± 8% of control) and area (93 ± 8%; both $P > 0.3$). Additionally, NIF had no significant effect on the amplitude (129 ± 14% of control), area (124 ± 22%) or frequency (132 ± 30%) of the XII motor output (all $P > 0.15$, $n = 4$, Fig. 5*A*).

Group I mGluRs contribute to rhythm-related burst generation by blocking K^+ currents that are active at subthreshold membrane potentials, causing transient depolarization in lamprey spinal neurons (Kettunen *et al.* 2003) and in neonatal mice XII motoneurons (Sharifullina *et al.* 2004). We tested whether group I mGluRs were coupled to K^+ channels in preBötC neurons. When we blocked K^+ channels with a Cs^+-based patch solution, LY (15 μM) no longer caused significant reductions in inspiratory drive potentials; area and amplitude were 91 ± 5% and 80 ± 12% of control (both $P > 0.12$, $n = 5$, Figs 3*A* and 5*B*); in contrast, MPEP (10 μM) reduced the amplitude and area of the inspiratory drive potentials to 72 ± 5% and 45 ± 6% of control (both $P < 0.01$, $n = 3$, Figs 3*B* and 5*B*).

Group I mGluRs catalyse IP_3 production, which triggers intracellular Ca^{2+} release. We tested whether IP_3R-mediated intracellular Ca^{2+} release plays a role in

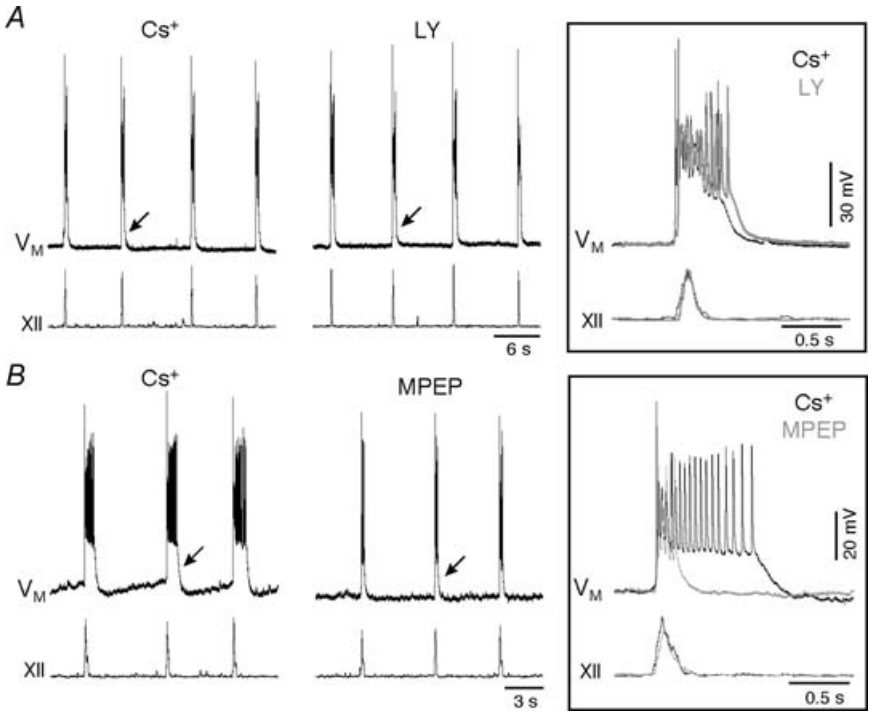

Figure 3. Evaluating whether mGluRs act via K^+ channels
A, inspiratory bursts were transformed into inspiratory plateau potentials by intracellular Cs^+, which blocks the attenuating effects of LY367385 (LY; 15 μM). *B*, MPEP (10 μM) attenuates Cs^+-induced inspiratory plateau potentials. In *A* and *B*, arrows indicate inspiratory bursts shown at high time resolution in the insets at right. Voltage calibration bars in the insets apply to all traces in *A* and *B*. Individual time calibration bars are illustrated for traces and insets. Baseline membrane potential was –60 mV.

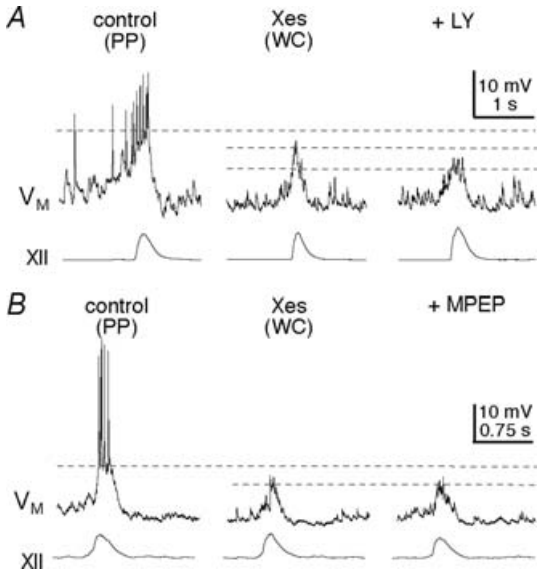

Figure 4. Role of IP_3 signalling in inspiratory bursts
A, nystatin perforated-patch recordings served as control. The IP_3R antagonist xestospongin (Xes; 1 μM), applied intracellularly by patch rupture, reduces inspiratory bursts. Subsequent bath application of LY367385 (LY; 15 μM) additionally attenuates inspiratory bursts. *B*, same protocol as *A*, except that MPEP, and not LY, is bath applied in steady-state Xes conditions. MPEP has no additional effects on inspiratory bursts. Baseline membrane potential was −60 mV. *A* and *B* have separate calibration bars as shown.

drive potential generation by intracellular application of the IP_3R antagonist xestospongin-C (Xes; 1 μM) (Gafni *et al.* 1997). We used nystatin-perforated patches to measure drive potentials in control (e.g. Fig. 1*B*), then we ruptured the membrane to obtain whole-cell conditions; within 6–10 min, intracellular Xes reduced the amplitude and area of drive potentials to $67 \pm 5\%$ and $64 \pm 6\%$ of control, respectively (both $P < 0.001$, $n = 16$, Figs 4 and 5*A*).

If group I mGluRs act exclusively through IP_3-dependent Ca^{2+} release, then blocking either receptor (mGluR1 or mGluR5) after dialysis with Xes should not have any additional effect on the inspiratory drive potential. In the presence of intracellular Xes, LY (15 μM) significantly attenuated the amplitude and area of the drive potential to $71 \pm 6\%$ and $68 \pm 5\%$ of steady-state Xes conditions ($P < 0.05$, $n = 4$, Figs 4*A* and 5*B*), which suggests that mGluR1 acts independently of IP_3Rs. In contrast, MPEP (10 μM) had no effect on drive potentials in the presence of intracellular Xes; the amplitude and area of drive potentials remained at $100 \pm 12\%$ and $99 \pm 19\%$ of steady-state Xes conditions ($P > 0.5$, $n = 3$, Figs 4*B* and 5*B*), which suggests that mGluR5 acts exclusively via IP_3Rs.

Intracellular Ca^{2+} signalling and inspiratory drive potential generation

NMDARs and IP_3Rs contribute to inspiratory drive potentials (Figs 2*A*, 4 and 5*A*) and utilize intracellular Ca^{2+} as a second messenger. Therefore, we tested the role of Ca^{2+} signalling using a high concentration of intracellular BAPTA (30 mM). Nystatin perforated patches were used to measure inspiratory drive in control (e.g. Fig. 1*B*). After rupturing the membrane and establishing whole-cell dialysis for ~20 min, BAPTA significantly decreased the amplitude and area of inspiratory drive potentials to $36 \pm 5\%$ and $42 \pm 7\%$ of control (both $P < 10^{-8}$, $n = 5$, Fig. 6*A* and *B*). In 24 additional experiments without nystatin we used the first 1 min of whole-cell recording as control and intracellular BAPTA yielded identical results; the amplitude and area of inspiratory drive potentials decreased to $32 \pm 3\%$ and $33 \pm 3\%$ of control (both $P < 10^{-9}$, $n = 24$, Fig. 6*B*).

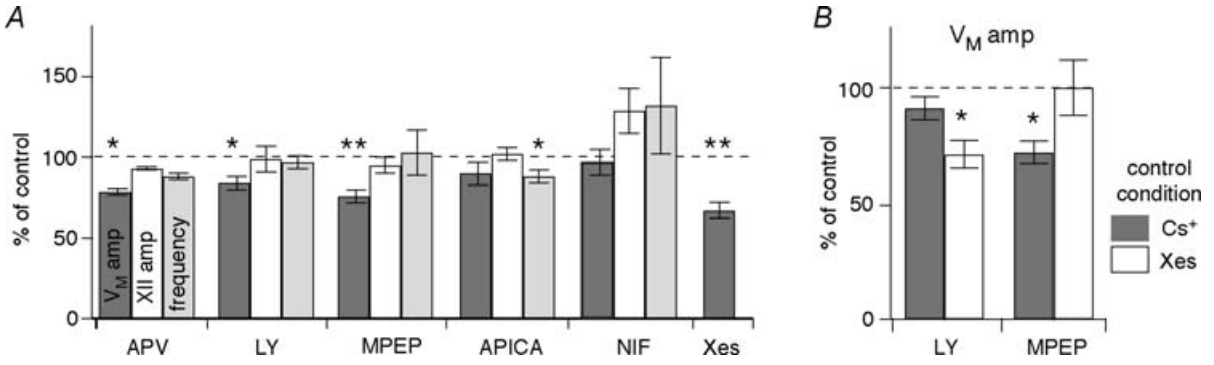

Figure 5. Summary of blocking glutamatergic and IP_3 receptors on drive potential generation
A, bar chart showing the effects of APV, LY367385 (LY), MPEP, APICA, nifedipine (NIF), and xestospongin-C (Xes) on the amplitude of drive potentials, as well as the amplitude and frequency of XII motor output. *B*, bar chart showing the effects of LY and MPEP on the amplitude of drive potentials in steady-state intracellular Cs^+ or Xes conditions. Asterisks above bars indicate significant effects at $P < 0.05$ (*) and $P < 0.01$ (**), respectively.

To examine whether resting $[Ca^{2+}]_i$ influenced inspiratory drive potentials, we formulated 30 mM BAPTA patch solutions with $[Ca^{2+}]_i$ buffered to nominally 0, 25 or 120 nM (see Methods). Baseline $[Ca^{2+}]_i$ had no significant effect on the BAPTA-mediated attenuation of drive potentials ($P > 0.25$ with regard to both amplitude and area, Fig. 6*C*). These results suggest that intracellular Ca^{2+} transients, but not the resting $[Ca^{2+}]_i$, affect drive potential generation. These data are consistent with intracellular Ca^{2+} transients activating an inward current that enhances inspiratory drive potentials. I_{CAN} is an obvious candidate.

I_{CAN} in preBötC neurons

I_{CAN} activation requires intracellular Ca^{2+} transients, which should be blocked by 30 mM intracellular BAPTA. To test whether BAPTA was in fact blocking I_{CAN}, we bath-applied the I_{CAN} antagonist FFA (100 μM, > 15 min) after 30 mM BAPTA reached steady-state conditions ($\geq$ 30 min), which avoids falsely attributing the effects of 30 mM BAPTA to bath-applied 100 μM FFA. Previously, we showed that 100 μM FFA attenuates drive potential generation in preBötC neurons (Del Negro *et al.* 2005). Here in the presence of intracellular BAPTA, we found that 100 μM FFA had no effect on the amplitude (131 ± 22% of control) or area (129 ± 17% of control) of inspiratory drive potentials (both $P > 0.3$, $n = 5$, Fig. 6*A* and *B*). This suggests that both BAPTA and FFA (100 μM) act on the same mechanism, consistent with I_{CAN}.

Next, we quantified the effects of bath application of FFA (10, 100, 300 and 350 μM) on drive potential generation and XII motor output. FFA at 10 μM (15 min) had no significant effect on the amplitude (86 ± 8% of control) or area (88 ± 13%) of inspiratory drive potentials nor on the amplitude (106 ± 11%), area (112 ± 18%) or frequency of XII motor output (98 ± 3%) (all $P > 0.25$, $n = 4$, not shown). At 100 μM, FFA reduced drive potential amplitude and area significantly to 70 ± 5% ($P < 0.01$) and 65 ± 10% ($P < 0.05$) of control. FFA at 100 μM had no effect on the amplitude (79 ± 11%), area (89 ± 11%) or frequency (89 ± 13%) of XII motor output (all $P > 0.18$, $n = 6$, Fig. 7*A*). Note that the actions of 100 μM FFA reached steady state in ~12 min and its effects on inspiratory drive potentials were not fully reversible.

In contrast, 300 μM FFA caused rhythm cessation after 10–15 min in 7 of 10 slices tested (Fig. 7*B*). In the remaining 3 slices, raising the concentration of FFA to 350 μM silenced the rhythm (Fig. 7*C*). In all cases, XII motor output was never revived by adding 1 μM of the excitatory neuropeptide substance P (SP, bath-applied > 10 min) but recovered in washout ($n = 10$, Fig. 7*C*).

The FFA-sensitive current in preBötC neurons has been attributed to I_{CAN} (Peña *et al.* 2004), but this issue is not yet fully resolved. FFA also affects gap junctions and Ca^+-dependent K^+ channels (Ottolia & Toro, 1994; Greenwood & Large, 1995; Kochetkov *et al.* 2000; Harks *et al.* 2001). To verify the presence of I_{CAN} in preBötC

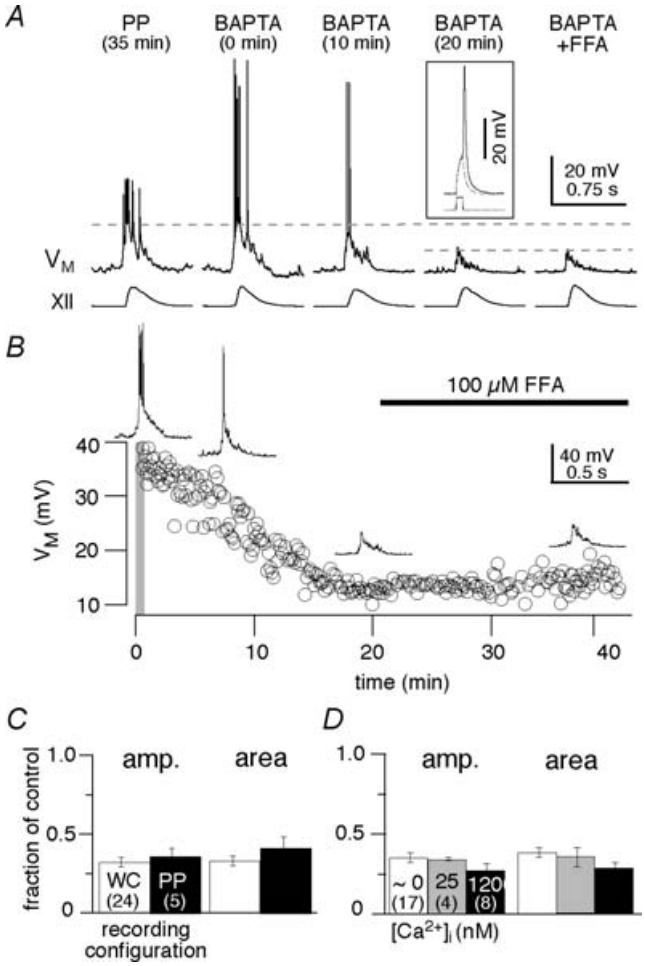

Figure 6. Intracellular Ca^{2+} transients are important for inspiratory bursts
A, perforated-patch recordings and intracellular dialysis using 30 mM BAPTA patch solution. Control conditions in the perforated-patch configuration are shown at 35 min. BAPTA once introduced into the cytosol via patch rupture causes a progressive attenuation of the inspiratory burst. Inset shows that action potentials could be evoked with 5 ms-long current pulses (at rheobase) in steady-state intracellular BAPTA conditions (> 20 min). Subsequent bath-application of 100 μM flufenamic acid (FFA) has no additional attenuating effects even after 15 min of exposure to the drug. Baseline membrane potential was –60 mV throughout the experiment. *B*, time course of the effects of 30 mM BAPTA on the amplitude of inspiratory bursts (V_M). The first minute of whole-cell configuration is indicated by the grey bar at zero time. Subsequent bath-application of 100 μM FFA causes no additional attenuation. *C*, bar chart showing that BAPTA reduces both the amplitude (amp.) and area of inspiratory drive potentials to the same extent whether WC ($n = 24$) or PP ($n = 5$) recording configurations are used for control. *D*, patch solutions that buffered baseline $[Ca^{2+}]_i$ to nominally 0 ($n = 17$), 25 ($n = 4$), or 120 nM ($n = 8$) have no significant effect on the BAPTA-mediated attenuation of inspiratory drive potential amplitude or area. *C* and *D* show mean ± S.E.M., and number of experiments in parentheses.

neurons we tested for its hallmark properties: activation by intracellular Ca^{2+}, with Na^+ as the primary inward charge carrier (Teulon, 2000). To isolate the effects of Na^+ substitution on putative I_{CAN}, we bath-applied 1 μM TTX, which also blocks rhythmogenesis in the slice. Therefore, we used a Cs^+-based patch-pipette solution and depolarizing current steps to reliably evoke I_{CAN}-mediated plateau-like potentials.

Intracellular Cs^+, which attenuates K^+ currents and reduces electrotonic length, transformed the inspiratory drive potential present in control into a long-lasting plateau potential (Fig. 8*A*, traces 1 and 2) that could also be evoked exogenously with a 50–150 ms current pulse (Fig. 8*A*, trace 3). The evoked plateaus were attenuated by 100 μM FFA ($n = 5$, Fig. 8*A*, traces 2–5) in a manner consistent with the effects of 100 μM FFA on endogenous drive potentials, e.g. Fig. 7*A*.

In 1 μM TTX, addition of Cd^{2+} (200 μM) to block Ca^{2+} influx attenuated the evoked plateau to $29 \pm 9\%$ of control ($P < 0.05$, $n = 3$); the subsequent equimolar replacement of Na^+ with choline caused no significant change in the evoked response (Fig. 8*B*, $n = 3$). Reversing the order of these tests, choline substitution attenuated the evoked plateau to $13 \pm 2\%$ of control ($P < 0.05$, $n = 3$); further addition of Cd^{2+} (200 μM) caused no further reduction (Fig. 8*C*, $n = 6$ total). Also in the presence of 1 μM TTX, 100 μM FFA attenuated the evoked plateau to $39 \pm 8\%$ of control ($P < 0.05$, $n = 6$). Choline substitution further reduced the response by an additional $31 \pm 11\%$ ($P < 0.05$, $n = 4$, Fig. 8*D*). These data indicate that I_{CAN} is expressed in preBötC neurons and is substantially, but incompletely, reduced by 100 μM FFA.

Discussion

Inspiratory drive potentials are a signature of preBötC neurons during the inspiratory phase of the respiratory cycle. We show that inspiratory drive potentials depend on both ionotropic and metabotropic glutamate receptors to evoke postsynaptic membrane properties. AMPARs are essential for respiratory rhythmogenesis (Greer *et al.* 1991; Funk *et al.* 1993; Ge & Feldman, 1998; Koshiya & Smith, 1999) and thus are pivotal for inspiratory drive potential generation *in vitro*. However, the roles of

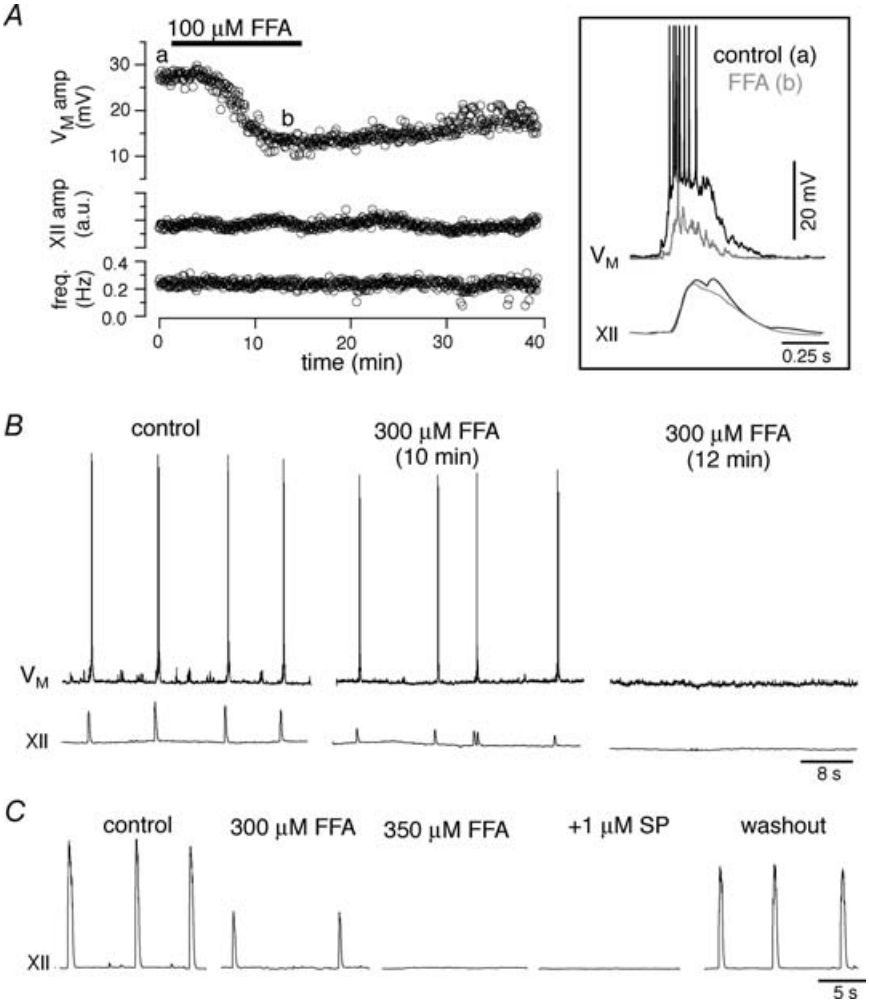

Figure 7. The I_{CAN} antagonist, flufenamic acid (FFA), attenuates inspiratory drive potentials
A, 100 μM FFA reduces drive potentials but not the magnitude or frequency of XII motor discharge. The letters 'a' and 'b' indicate inspiratory bursts that are shown at high resolution in the inset (at right) for control (a) and 100 μM FFA (b). *B*, 300 μM FFA blocks inspiratory activity in 7 of 10 slices after 12 or more minutes of drug exposure. *C*, in the 3 remaining slices, 350 μM FFA blocks the respiratory rhythm, which does not restart in the presence of 1 μM substance P (SP), but does recover after > 1 h of washout. Baseline membrane potential was −60 mV for V_M traces in *A* (inset) and *B*. *A* (inset), *B* and *C* all have separate time calibrations.

NMDARs and mGluRs in drive potential generation have largely been overlooked. We show that both NMDARs and group I mGluRs contribute significantly to inspiratory drive potential generation. Inspiratory drive potentials required intracellular Ca^{2+} transients and decreased after exposure to 100 μM FFA. This suggests that I_{CAN} is involved in inspiratory drive potential generation.

Additionally, evoked plateau potentials under intracellular Cs^+ conditions were attenuated by FFA and also sensitive to external Na^+ substitution and Cd^{2+}, which is indicative of I_{CAN}. These properties are also hallmarks of unconventional members of the *transient receptor potential*, i.e. TRP, family of ion channels, namely TRPM4 and/or TRPM5, which are FFA-sensitive, monovalent cation channels gated by intracellular Ca^{2+}. Therefore TRPM4 and/or TRPM5 may underlie I_{CAN} in preBötC neurons (Launay *et al.* 2002; Hofmann *et al.* 2003; Montell, 2005; Ullrich *et al.* 2005).

Role of I_{CAN} in inspiratory drive potentials and respiratory rhythmogenesis

Testing the role of I_{CAN} in inspiratory drive potential generation using FFA proved difficult. At 100 μM, FFA incompletely blocked I_{CAN} (Fig. 8*D* and Teulon, 2000) whereas higher concentrations stopped respiratory rhythmogenesis altogether. Although it is tempting to conclude that FFA at doses of 300–350 μM, e.g. Fig. 7*B*, stopped the rhythm by fully blocking I_{CAN}, FFA at concentrations exceeding 100 μM significantly affects gap junctions, Ca^+-dependent K^+ channels and Cl^- channels (Ottolia & Toro, 1994; Greenwood & Large, 1995; Kochetkov *et al.* 2000; Harks *et al.* 2001), which are present in preBötC neurons (Rekling & Feldman, 1997*a*; Brockhaus & Ballanyi, 1998; Onimaru *et al.* 2003). Therefore, here and elsewhere, e.g. (Peña *et al.* 2004; Tryba *et al.* 2006), whether FFA is applied alone or in

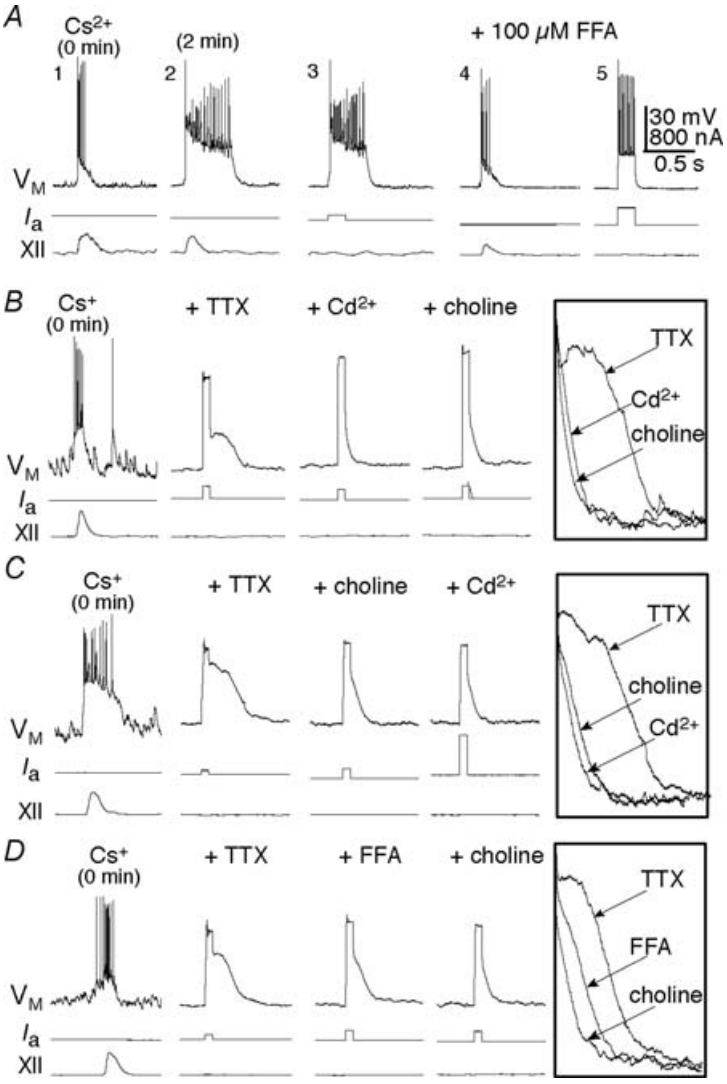

Figure 8. The ionic basis of I_{CAN}
A, preBötC neuron recorded with Cs^+-patch solution shown immediately after onset of whole-cell recording (*A,* trace 1). After 2 min, the drive potential is transformed into an inspiratory plateau response (2), which can also be evoked using 150 ms somatic current pulses (3). At 100 μM FFA reduces the endogenous (4) and evoked (5) responses. *B*, inspiratory plateaus evoked with 50 ms current steps were subjected to cumulative applications of 1 μM TTX, 200 μM Cd^{2+} and choline substitution for Na^+ in the ACSF. Inset shows superimposition of the active responses immediately following current-pulse stimuli. *C*, inspiratory plateaus subjected to the same agents as in *B* (above), but with Cd^{2+} and choline substitution in reverse order. Inset is similarly constructed. *D*, inspiratory plateaus subjected to 1 μM TTX, and then cumulatively followed by 100 μM FFA and choline substitution. Inset is similarly constructed to *B* and *C*. Calibration bars in *A* apply to *A–D* and baseline membrane potential was −60 mV.

combination with other drugs, one cannot assert that rhythm cessation brought on by FFA at doses exceeding 100 μM is attributable solely to the ability of FFA to block of I_{CAN}.

How are we to reconcile our finding that 300–350 μM FFA blocks rhythm generation with the prior report by Peña *et al.* (2004) in which 500 μM FFA was bath-applied and failed to stop respiratory rhythm in slices? This apparent discrepancy can be explained as follows: the duration of FFA application is an important parameter because we found dramatic effects of FFA within a 2 min window, e.g. Fig. 7*B*, during which the rhythm went from normal frequency to complete stoppage. The time course of FFA application was not specified in Peña *et al.* (pertaining to their Fig. 7*B*) thus one cannot evaluate whether FFA reached steady state in their protocol. Moreover, the slices employed by Peña *et al.* were 630–690 μm thick with their rostral surface at the caudal pole of the facial nucleus (see Methods in Peña *et al.* 2004), which suggests that critical preBötC rhythmogenic neurons were located ~200 μm deeper within their tissue compared to our slices and thus would probably require longer exposure times for FFA to achieve its steady-state effects. Lastly, one cannot rule out that rostral rhythmogenic circuits located at the caudal pole of the facial nucleus such as the retrotrapezoid-parafacial respiratory group (RTN-pFRG) (Onimaru & Homma, 2003; Janczewski & Feldman, 2006) may be present in the slices in Peña *et al.*, as suggested by the likely cytoarchitectonic boundaries (Ruangkittisakul *et al.* 2006; Barnes *et al.* 2007). In contrast, the RTN-pFRG is not present in our slices, which isolates the preBötC at the rostral surface (see Methods and Ruangkittisakul *et al.* 2006).

To address the pharmacological caveats associated with use of FFA, we straightforwardly analysed the role of I_{CAN} in inspiratory drive potential generation using high levels of intracellular BAPTA, which prevented I_{CAN} activation by suppressing Ca^{2+} transients. BAPTA at 30 mM appears to substantially, if not quite fully, block I_{CAN} yet has few (if any) other effects on burst generation or membrane properties. For example: inspiratory drive potentials were not further attenuated following intracellular BAPTA dialysis by the subsequent application of 100 μM FFA. Also, 30 mM BAPTA had no effect on input resistance and did not affect action potentials evoked with current pulses (Fig. 6*A* inset). To the extent that BAPTA dialysis affects Ca^{2+}-dependent K^+ channels that normally attenuate the magnitude of inspiratory drive potentials (Onimaru *et al.* 2003), we expect that the 60–70% BAPTA-mediated attenuation may actually underestimate the true contribution of I_{CAN} during inspiratory drive potentials. We conclude that I_{CAN} predominantly contributes to inspiratory drive on a cycle-to-cycle basis by significantly boosting the transformation of glutamatergic synaptic inputs to membrane depolarization.

I_{CAN} activation mechanisms in preBötC neurons

We hypothesize that three pathways normally activate I_{CAN} during inspiratory drive potential generation. First, synaptically activated mGluR5s trigger IP_3-mediated intracellular Ca^{2+} release, which activates I_{CAN}. A similar mechanism may promote network-driven oscillations in CA1 pyramidal neurons, where group I mGluRs activate I_{CAN} via a mechanism that probably involves IP_3-mediated Ca^{2+} release (Congar *et al.* 1997).

Second, inspiratory drive potentials depended on NMDAR-mediated Ca^{2+} influx, which may play a small but statistically significant role in activating I_{CAN}. While the burst-generating role of NMDARs is small in preBötC neurons, Ca^{2+} influx through NMDARs exclusively activates I_{CAN} to generate bursting oscillations in subthalamic neurons (Zhu *et al.* 2004*a*,*b*). AMPARs are primarily Ca^{2+} impermeable in preBötC neurons (Paarmann *et al.* 2000) and thus probably cannot activate I_{CAN} directly.

Third, ionotropic receptor-mediated depolarization due to AMPARs, and possibly NMDARs, opens voltage-gated Ca^{2+} channels (Frermann *et al.* 1999; Pierrefiche *et al.* 1999; Onimaru & Homma, 2003) and directly activates I_{CAN} (Fig. 8*B* and Peña *et al.* 2004). Voltage-gated Ca^{2+} channels recruited by synaptic depolarization activate I_{CAN} in motoneurons of the nucleus ambiguous (Rekling & Feldman, 1997*b*), layer II neurons in the entorhinal cortex (Egorov *et al.* 2002; Fransen *et al.* 2006), and Blanes cells of the olfactory bulb (Pressler & Strowbridge, 2006). Importantly, in neocortical slices NMDARs, voltage-gated Ca^{2+} channels and intracellular Ca^{2+} release all converge to activate I_{CAN} during epileptiform discharges (Schiller, 2004), which resemble a prolonged version of the inspiratory drive potentials in preBötC neurons.

Rather than acting on I_{CAN}, mGluR1 appears to promote inspiratory drive potentials by transiently closing K^+ channels. A similar role for mGluR1 was identified in lamprey spinal neurons and neonatal mice XII motoneurons, in which mGluR1-modulated K^+ leak channels boost membrane depolarization and increase membrane excitability *in vitro* (Kettunen *et al.* 2003; Sharifullina *et al.* 2004).

The specific subtype of Ca^{2+} channel involved in I_{CAN} activation in preBötC neurons remains unknown. While L-type Ca^{2+} channels are present in preBötC neurons (Onimaru *et al.* 1996, 2003; Mironov & Richter, 1998; Elsen & Ramirez, 2005) and are regulated by group I mGluR activation (Mironov & Richter, 2000), they do not contribute to drive potential generation or XII motor

output under standard conditions *in vitro* (Fig. 5*A* and Onimaru *et al.* 2003). However, the role of L-type Ca^{2+} channels may change during hypoxia (Mironov & Richter, 2000).

Onimaru *et al.* (1996, 2003) studied N-type and P/Q-type Ca^{2+} channels in respiratory neurons throughout the ventral medullary column, including the RTN-pFRG. N-type Ca^{2+} channel blockade actually increases the magnitude of inspiratory drive potentials because these channels are functionally linked to SK-type Ca^{2+}-dependent K^+ channels, and the net effect of blocking them is to remove an activity-dependent outward current (Onimaru *et al.* 2003). In contrast, ω-agatoxin-IVA bath application significantly reduces inspiratory drive potential amplitude (Onimaru *et al.* 2003), which suggests that P/Q-type Ca^{2+} channels may participate in I_{CAN} activation, although this remains to be demonstrated in preBötC neurons specifically.

That AMPARs are critical for rhythm generation may simply reflect their role as the primary source of excitatory postsynaptic currents during the inspiratory phase. However, NMDAR, mGluR1 and mGluR5 antagonists significantly attenuated the magnitude of inspiratory drive potentials (Fig. 2), which suggests that the bulk of the inward current during inspiratory drive is not conveyed by AMPARs. To explain their critical role *in vitro*, we posit that AMPARs recruit and initiate the mechanisms that activate I_{CAN}. These mechanisms include the AMPAR-mediated depolarization required to activate Ca^{2+} channels and partially relieve the voltage-dependent Mg^{2+} block of NMDARs.

Physiological significance

One might expect that reducing the magnitude of drive potentials in preBötC neurons would necessarily result in decreased XII motor output, whereas in most of our experiments XII motor output was maintained even though drive potentials in preBötC neurons decreased significantly. At present, how changes in the inspiratory drive potentials from preBötC neurons affect presynaptic drive to XII motoneurons is unknown. However, inspiratory synaptic drive to XII motoneurons is primarily AMPAR mediated with little to no postsynaptic contribution from NMDARs (Funk *et al.* 1993) or mGluRs (Bocchiaro & Feldman, 2004; Sharifullina *et al.* 2004; Nistri *et al.* 2006). Therefore, the pharmacological approaches used in this study to attenuate inspiratory drive in the preBötC should not have affected XII motoneurons directly. In contrast, XII motoneurons express persistent Na^+ current (I_{NaP}) (Bellingham, 2006), which is consistent with bath-applied riluzole, the I_{NaP} antagonist, causing dose-dependent decreases in XII motor nerve output (Del Negro *et al.* 2002*b*, 2005) that is not seen when riluzole was injected directly into the preBötC (Pace *et al.* 2007).

We conclude that I_{CAN} predominantly contributes to inspiratory drive on a cycle-to-cycle basis by augmenting the transformation of synaptic input to membrane depolarization. I_{CAN} only becomes fully activated by glutamate-mediated activation of AMPA, NMDA and metabotropic glutamate receptors during endogenous respiratory behaviour, and thus is properly considered a network-induced property (and would not be activated by current injection via an intracellular or patch electrode). A rhythmogenic mechanism that depends on glutamatergic recurrent excitation coupled to intrinsic burst-generating currents via intracellular signalling mechanisms was predicted by Rekling and colleagues and dubbed the *group pacemaker hypothesis* (Rekling *et al.* 1996; Rekling & Feldman, 1998). In the group pacemaker hypothesis, some or all preBötC neurons express postsynaptic currents that are normally latent and unavailable except when recruited by synaptically activated signalling cascades. This is a major paradigm shift because the rhythmogenic population need not express intrinsic voltage-dependent pacemaker properties to play a key role in inspiratory burst generation. In light of the diminishing evidence in support of the *obligatory* role of pacemaker properties in respiratory rhythm generation (Del Negro *et al.* 2005; Pace *et al.* 2007), our findings demonstrate that a framework in which recurrent synaptic excitation evokes cellular burst-generating membrane properties available to all preBötC neurons, such as the group pacemaker hypothesis, is a viable mechanism that can explain key aspects of respiratory rhythmogenesis.

References

Attwell D & Gibb A (2005). Neuroenergetics and the kinetic design of excitatory synapses. *Nat Rev Neurosci* **6**, 841–849.

Barnes BJ, Tuong CM & Mellen NM (2007). Functional imaging reveals respiratory network activity during hypoxic and opioid challenge in the neonate rat tilted sagittal slab preparation. *J Neurophysiol* **97**, 2283–2292.

Bellingham M (2006). Riluzole decreases synaptic excitation and repetitive firing in rat hypoglossal motor neurons. *Society for Neuroscience Annual Meeting: Neuroscience 2006*, *Atlanta, GA, USA*. 237.235.

Bocchiaro CM & Feldman JL (2004). Synaptic activity-independent persistent plasticity in endogenously active mammalian motoneurons. *Proc Natl Acad Sci U S A* **101**, 4292–4295.

Brockhaus J & Ballanyi K (1998). Synaptic inhibition in the isolated respiratory network of neonatal rats. *Eur J Neurosci* **10**, 3823–3839.

Canepari M, Papageorgiou G, Corrie JE, Watkins C & Ogden D (2001). The conductance underlying the parallel fibre slow EPSP in rat cerebellar Purkinje neurones studied with photolytic release of L-glutamate. *J Physiol* **533**, 765–772.

Congar P, Leinekugel X, Ben-Ari Y & Crepel V (1997). A long-lasting calcium-activated nonselective cationic current is generated by synaptic stimulation or exogenous activation of group I metabotropic glutamate receptors in CA1 pyramidal neurons. *J Neurosci* **17**, 5366–5379.

Del Negro CA, Koshiya N, Butera RJ Jr & Smith JC (2002*a*). Persistent sodium current, membrane properties and bursting behavior of pre-bötzinger complex inspiratory neurons in vitro. *J Neurophysiol* **88**, 2242–2250.

Del Negro CA, Morgado-Valle C & Feldman JL (2002*b*). Respiratory rhythm: an emergent network property? *Neuron* **34**, 821–830.

Del Negro CA, Morgado-Valle C, Hayes JA, Mackay DD, Pace RW, Crowder EA & Feldman JL (2005). Sodium and calcium dependent pacemaker neurons and respiratory rhythm generation. *J Neurosci* **25**, 446–453.

Egorov AV, Hamam BN, Fransen E, Hasselmo ME & Alonso AA (2002). Graded persistent activity in entorhinal cortex neurons. *Nature* **420**, 173–178.

Elsen FP & Ramirez JM (2005). Postnatal development differentially affects voltage-activated calcium currents in respiratory rhythmic versus nonrhythmic neurons of the pre-Bötzinger complex. *J Neurophysiol* **94**, 1423–1431.

Feldman JL & Del Negro CA (2006). Looking for inspiration: new perspectives on respiratory rhythm. *Nat Rev Neurosci* **7**, 232–241.

Ferraguti F & Shigemoto R (2006). Metabotropic glutamate receptors. *Cell Tissue Res* **326**, 483–504.

Fransen E, Tahvildari B, Egorov AV, Hasselmo ME & Alonso AA (2006). Mechanism of graded persistent cellular activity of entorhinal cortex layer v neurons. *Neuron* **49**, 735–746.

Frermann D, Keller BU & Richter DW (1999). Calcium oscillations in rhythmically active respiratory neurones in the brainstem of the mouse. *J Physiol* **515**, 119–131.

Funk GD, Johnson SM, Smith JC, Dong XW, Lai J & Feldman JL (1997). Functional respiratory rhythm generating networks in neonatal mice lacking NMDAR1 gene. *J Neurophysiol* **78**, 1414–1420.

Funk GD, Smith JC & Feldman JL (1993). Generation and transmission of respiratory oscillations in medullary slices: role of excitatory amino acids. *J Neurophysiol* **70**, 1497–1515.

Funk GD, Smith JC & Feldman JL (1995). Modulation of neural network activity in vitro by cyclothiazide, a drug that blocks desensitization of AMPA receptors. *J Neurosci* **15**, 4046–4056.

Gafni J, Munsch JA, Lam TH, Catlin MC, Costa LG, Molinski TF & Pessah IN (1997). Xestospongins: potent membrane permeable blockers of the inositol 1,4,5-trisphosphate receptor. *Neuron* **19**, 723–733.

Ge Q & Feldman JL (1998). AMPA receptor activation and phosphatase inhibition affect neonatal rat respiratory rhythm generation. *J Physiol* **509**, 255–266.

Greenwood IA & Large WA (1995). Comparison of the effects of fenamates on Ca-activated chloride and potassium currents in rabbit portal vein smooth muscle cells. *Br J Pharmacol* **116**, 2939–2948.

Greer JJ, Smith JC & Feldman JL (1991). Role of excitatory amino acids in the generation and transmission of respiratory drive in neonatal rat. *J Physiol* **437**, 727–749.

Harks EG, de Roos AD, Peters PH, de Haan LH, Brouwer A, Ypey DL, van Zoelen EJ & Theuvenet AP (2001). Fenamates: a novel class of reversible gap junction blockers. *J Pharmacol Exp Ther* **298**, 1033–1041.

Hofmann T, Chubanov V, Gudermann T & Montell C (2003). TRPM5 is a voltage-modulated and Ca^{2+}-activated monovalent selective cation channel. *Curr Biol* **13**, 1153–1158.

Janczewski WA & Feldman JL (2006). Distinct rhythm generators for inspiration and expiration in the juvenile rat. *J Physiol* **570**, 407–420.

Kettunen P, Hess D & El Manira A (2003). mGluR1, but not mGluR5, mediates depolarization of spinal cord neurons by blocking a leak current. *J Neurophysiol* **90**, 2341–2348.

Kochetkov KV, Kazachenko VN & Marinov BS (2000). Dose-dependent potentiation and inhibition of single Ca^{2+}-activated K^+ channels by flufenamic acid. *Membr Cell Biol* **14**, 285–298.

Koshiya N & Smith JC (1999). Neuronal pacemaker for breathing visualized in vitro. *Nature* **400**, 360–363.

Launay P, Fleig A, Perraud AL, Scharenberg AM, Penner R & Kinet JP (2002). TRPM4 is a Ca^{2+}-activated nonselective cation channel mediating cell membrane depolarization. *Cell* **109**, 397–407.

Lieske SP & Ramirez JM (2006). Pattern-specific synaptic mechanisms in a multifunctional network. II. Intrinsic modulation by metabotropic glutamate receptors. *J Neurophysiol* **95**, 1334–1344.

Mironov SL & Richter DW (1998). L-type Ca^{2+} channels in inspiratory neurones of mice and their modulation by hypoxia. *J Physiol* **512**, 75–87.

Mironov SL & Richter DW (2000). Hypoxic modulation of L-type Ca^{2+} channels in inspiratory brainstem neurones: intracellular signalling pathways and metabotropic glutamate receptors. *Brain Res* **869**, 166–177.

Montell C (2005). The TRP superfamily of cation channels. *Sci STKE* **2005**, re3.

Nistri A, Ostroumov K, Sharifullina E & Taccola G (2006). Tuning and playing a motor rhythm: how metabotropic glutamate receptors orchestrate generation of motor patterns in the mammalian central nervous system. *J Physiol* **572**, 323–334.

Onimaru H, Ballanyi K & Homma I (2003). Contribution of Ca^{2+}-dependent conductances to membrane potential fluctuations of medullary respiratory neurons of newborn rats in vitro. *J Physiol* **552**, 727–741.

Onimaru H, Ballanyi K & Richter DW (1996). Calcium-dependent responses in neurons of the isolated respiratory network of newborn rats. *J Physiol* **491**, 677–695.

Onimaru H & Homma I (2003). A novel functional neuron group for respiratory rhythm generation in the ventral medulla. *J Neurosci* **23**, 1478–1486.

Ottolia M & Toro L (1994). Potentiation of large conductance KCa channels by niflumic, flufenamic, and mefenamic acids. *Biophys J* **67**, 2272–2279.

Paarmann I, Frermann D, Keller BU & Hollmann M (2000). Expression of 15 glutamate receptor subunits and various splice variants in tissue slices and single neurons of brainstem nuclei and potential functional implications. *J Neurochem* **74**, 1335–1345.

Paarmann I, Frermann D, Keller BU, Villmann C, Breitinger HG & Hollmann M (2005). Kinetics and subunit composition of NMDA receptors in respiratory-related neurons. *J Neurochem* **93**, 812–824.

Pace RW, Mackay DD, Feldman JL & Del Negro CA (2007). Role of persistent sodium current in mouse preBotzinger Complex neurons and respiratory rhythm generation. *J Physiol* **580**, 485–496.

Partridge LD & Valenzuela CF (1999). Ca^{2+} store-dependent potentiation of Ca^{2+}-activated non-selective cation channels in rat hippocampal neurones in vitro. *J Physiol* **521**, 617–627.

Patneau DK, Mayer ML, Jane DE & Watkins JC (1992). Activation and desensitization of AMPA/kainate receptors by novel derivatives of willardiine. *J Neurosci* **12**, 595–606.

Peña F, Parkis MA, Tryba AK & Ramirez JM (2004). Differential contribution of pacemaker properties to the generation of respiratory rhythms during normoxia and hypoxia. *Neuron* **43**, 105–117.

Pierrefiche O, Haji A, Bischoff A & Richter DW (1999). Calcium currents in respiratory neurons of the cat in vivo. *Pflugers Arch* **438**, 817–826.

Pressler RT & Strowbridge BW (2006). Blanes cells mediate persistent feedforward inhibition onto granule cells in the olfactory bulb. *Neuron* **49**, 889–904.

Rekling JC, Champagnat J & Denavit-Saubie M (1996). Electroresponsive properties and membrane potential trajectories of three types of inspiratory neurons in the newborn mouse brain stem in vitro. *J Neurophysiol* **75**, 795–810.

Rekling JC & Feldman JL (1997*a*). Bidirectional electrical coupling between inspiratory motoneurons in the newborn mouse nucleus ambiguus. *J Neurophysiol* **78**, 3508–3510.

Rekling JC & Feldman JL (1997*b*). Calcium-dependent plateau potentials in rostral ambiguus neurons in the newborn mouse brain stem in vitro. *J Neurophysiol* **78**, 2483–2492.

Rekling JC & Feldman JL (1998). Preötzinger complex and pacemaker neurons: hypothesized site and kernel for respiratory rhythm generation. *Annu Rev Physiol* **60**, 385–405.

Ruangkittisakul A, Schwarzacher SW, Secchia L, Poon BY, Ma Y, Funk GD & Ballanyi K (2006). High sensitivity to neuromodulator-activated signaling pathways at physiological $[K^+]$ of confocally imaged respiratory center neurons in on-line-calibrated newborn rat brainstem slices. *J Neurosci* **26**, 11870–11880.

Sakmann B & Neher E (1995). *Single-Channel Recording*. Plenum Press, New York.

Schiller Y (2004). Activation of a calcium-activated cation current during epileptiform discharges and its possible role in sustaining seizure-like events in neocortical slices. *J Neurophysiol* **92**, 862–872.

Sharifullina E, Ostroumov K & Nistri A (2004). Activation of group I metabotropic glutamate receptors enhances efficacy of glutamatergic inputs to neonatal rat hypoglossal motoneurons in vitro. *Eur J Neurosci* **20**, 1245–1254.

Smith JC, Ellenberger HH, Ballanyi K, Richter DW & Feldman JL (1991). Pre-Bötzinger complex: a brainstem region that may generate respiratory rhythm in mammals. *Science* **254**, 726–729.

Stuart G, Spruston N & Häusser M (1999). *Dendrites*. Oxford University Press, Oxford, New York.

Teulon J (2000). Ca^{2+}-activated nonselective cation channels. In *Pharmacology of Ionic Channel Function: Activators and Inhibitors*, ed.Endo M, Kurachi Y, Mishina M, pp. 625–649. Springer-Verlag, Berlin.

Trussell LO & Fischbach GD (1989). Glutamate receptor desensitization and its role in synaptic transmission. *Neuron* **3**, 209–218.

Trussell LO, Zhang S & Raman IM (1993). Desensitization of AMPA receptors upon multiquantal neurotransmitter release. *Neuron* **10**, 1185–1196.

Tryba AK, Peña F & Ramirez JM (2006). Gasping activity *in vitro*: A rhythm dependent on 5-HT_{2A} receptors. *J Neurosci* **26**, 2623–2634.

Ullrich ND, Voets T, Prenen J, Vennekens R, Talavera K, Droogmans G & Nilius B (2005). Comparison of functional properties of the Ca^{2+}-activated cation channels TRPM4 and TRPM5 from mice. *Cell Calcium* **37**, 267–278.

Zhu ZT, Munhall A, Shen KZ & Johnson SW (2004*a*). Calcium-dependent subthreshold oscillations determine bursting activity induced by *N*-methyl-D-aspartate in rat subthalamic neurons in vitro. *Eur J Neurosci* **19**, 1296–1304.

Zhu ZT, Munhall A, Shen KZ & Johnson SW (2004*b*). Involvement of Ca^{2+}-activated nonselective cation conductance in potentiation of depolarization-gated inward currents evoked by NMDA in subthalamic neurons. *Society for Neuroscience 34th Annual Meeting, San Diego, CA, USA*. 169.162.

Acknowledgements

This work was supported by National Science Foundation IOB-0616099 (USA), National Institutes of Health HL-40959 (USA), the Jeffress Memorial Trust (Richmond, Virginia, USA), and the Suzann Wilson Matthews Faculty Research Award (The College of William and Mary, Williamsburg, Virginia, USA). We thank John A. Hayes for assistance with data acquisition, analysis, and consultation with the manuscript.

Supplemental material

Online supplemental material for this paper can be accessed at:
http://jp.physoc.org/cgi/content/full/jphysiol.2007.133660/DC1
and
http://www.blackwell-synergy.com/doi/suppl/10.1113/jphysiol.2007.133660